Hindawi
Advances in Materials Science and Engineering
Volume 2021, Article ID 9961590, 21 pages
https://doi.org/10.1155/2021/9961590

Research Article

Experimental Investigation of Dry and Cryogenic Friction Stir Welding of AA7075 Aluminium Alloy

A. Praveen Raj Navukkarasan,[1] **K. Shanmuga Sundaram**,[1] **C. Chandrasekhara Sastry**,[2] **and M. A. Muthu Manickam**[3]

[1]*Department of Mechanical Engineering, CEG Main Campus of Anna University, Chennai, India*
[2]*Department of Mechanical Engineering, Indian Institute of Information Technology, Design and Manufacturing (IIIT,D & M), Kurnool 518 007, Andhra Pradesh, India*
[3]*Combat Vehicles Research & Development Establishment, Defence R&D Organization (DRDO), Govt. of India, Ministry of Defence, Delhi, India*

Correspondence should be addressed to A. Praveen Raj Navukkarasan; praveencegau@gmail.com

Received 3 April 2021; Revised 28 April 2021; Accepted 30 August 2021; Published 21 September 2021

Academic Editor: Gianfranco Palumbo

An attempt has been made to investigate dry and cryogenic friction stir welding of AA 7075 aluminium alloy, which is predominantly availed in aerospace and defence component industries. These industries avail friction stir welding for joining two nonferrous materials, and minimal deviations and maximum strength are the preliminary and long time goal. A cryogenic friction stir welding setup was developed to conduct the joining of two aluminium alloy pipes. An increase of 0.76–42.93% and 3.79–31.24% in microhardness and tensile strength, respectively, is ascertained in cryogenic friction stir welding in correlation to dry friction stir welding of aluminium alloys. TOPSIS evaluation for the experimental run indicated tool profile stepped type, pipe rotation speed of 1000 rpm, welding speed of 50 mm/min, and axial force of 8 kN as close to unity ideal solution for dry and cryogenic friction stir welding of AA 7075 aluminium alloys. The friction stir-welded component under the cryogenic environment showcased drop in temperature, curtailed surface roughness, and fine grain structure owing to reduction in temperature differential occurring at the weld zone. A curtailment of 50.84% is ascertained in the roughness value for cryogenic friction stir welding in correlation to dry friction stir welding of AA 7075 alloy. A decrement of 21.68% is observed in the grain size in the cryogenic condition with correlation to the dry FSW process, indicating a drop in the coarse structure. With the curtailment of grain size and drop in temperature differential, compressive residual factor and corrosion resistance attenuated by 40.14% and 67.17% in the cryogenic FSW process in correlation to the dry FSW process, respectively.

1. Introduction

Aluminium alloy 7075 has been extensively availed in the areas of military vehicle armour materials, Earth excavating machines, bridges, aerospace components, and majority of the defence high-stressed applications [1]. The salient importance of this material is limited due to its welding properties as the fusion problem is predominant in 7075 aluminium series, i.e., porosity formation, solidification of hot cracked areas in the welded zone, and increase in the microfissuring aspect in the semipartially melted zone (SPMZ) [2–7]. The composition of AA 7075 aluminium alloy possesses copper, which does not have a specific melting point, and this creates a wide melting range for the alloy with a very low solidus temperature making it susceptible to hot cracks (welded zone) during fusion welding [1, 5, 8]. Friction stir welding (FSW) is a solid state welding method, availed to bring about joining of nonferrous materials such as aluminium, magnesium, copper, and steels [3–7, 9, 10]. FSW is the preferred joining process for high-strength aluminium alloys particularly 2xxx and 7xxx series as they are generally considered difficult-to-weld or

unweldable [2]. Major benefits of availing the FSW process is (i) limited weld defects, (ii) addressing aluminium welding capability (difficult to weld material classification for aluminium), and (iii) way better dimensional capability if the process occurs in a controlled manner. All these above are specific to FSW if the whole process is well maintained and run in an optimized condition [3–8, 10]. In this method of joining materials, a nonconsumable tool pin profile generates friction heat by rotating between the parent material, as indicated in Figure 1. The rotation of the tool ensures proper stirring effect and mixing of the materials in and around the tool pin; thus, with a combination of mechanical and thermal treatment, the welding process is completed [3–7, 9, 11].

Even though the parent material remains in its solid state, drawbacks are ascertained in the line or region of welding as it undergoes high levels of deformation [6, 10], causing an upsurge of unavoidable changes in the microstructure of the component leading to curtailment of mechanical properties [3, 4], coupled with aggrandizement of tensile residual stress [3, 5–7]. To address these, postweld treatments were carried out, by aging, solution treatment, and room temperature welding (long range of time) [2, 3, 8, 10]. Though posttreatments lead to a drop in the volume fraction of the residual tensile phase, microstructure changes are limited to the boundary lines; also, in terms of cost, time, and labour, it was considered to be laborious procedure physically and economically. An alternative method involved performing friction stir welding in a soluble oil coolant to drop the temperature differential, but an antiwelding property increase was ascertained due to the formation of sulphide aggregates curtailing the strength (shear) of the component [12]. Another major factor of oil coolants is in the area of formation of fumes and gases which when exposed in the welding environment causes long-term health deteriorations [13]. So, given the scenario, dry FSW was concluded to be a cleaner operation along with being cost effective in nature [5, 14].

Another area that has been unexplored is in the area of cryogenic friction stir welding (subzero welding) of aluminium alloys. Corresponding to enhanced surface properties, nil change to the composition and high strength of the tool profile are added factors to explore the application of cryogenics in the welding operation [12, 13, 15]. With a clear abundance availability of liquid helium, hydrogen, oxygen, and nitrogen, subzero liquid comprising of nitrogen is given the preference owing to the ratio of expansion and abundant supply present in the atmosphere [12, 13, 16–18].

Cryogenic welding finds a substantial drop in the tool workpiece interface owing to the subzero nature of the liquid, thus in turn causing a drop in temperature and retention of the lubricating medium [12, 13]. Also, having a high evaporation rate and causing no external or internal changes to the parent material highlights the importance of green manufacturing techniques in the welding scenario involving cryogenic liquid nitrogen [15, 19]. In the defence and aerospace sector, a number of components are mass produced; thus, minimal deviations and high strength welds are expected from the manufacturing sector. This creates more importance especially with the involvement of nonferrous alloys. In this work, an investigation is carried out for dry and cryogenic friction stir welding of AA 7075 aluminium alloy in which attributes of the welding operation are tool profile, pipe rotation speed, welding speed, and axial force in correlation to tensile strength and microhardness. The surface morphology, residual stress component, topographical analysis, and corrosion analysis of the welded surfaces are conducted to validate the welding (FSW) operation. The welding method parameters of the operation are highlighted in Figure 2.

2. Materials and Methods

2.1. Development of Cryogenic-Assisted Friction Stir Welding Operational Setup. A friction stir welding tool is placed on a tool holder (FSW setup), and the workpiece is held by the centre of the lathe. Elaborated experimental details of dry and cryogenic-assisted friction stir welding are depicted in Figure 3.

For conducting cryogenic-aided friction stir welding, a cryogenic setup was developed which is depicted in Figure 4 and tabulated in Table 1.

TA 55 liquid nitrogen container of 51.5 litres capacity is availed for the FSW cryogenic system. To retain the subzero fluid, a completely sealed aluminium container is availed with steel closure. Inlet of the pipes of size 6 mm and 4 mm is placed inside through the steel cap enclosure for the flow of compressed air and the outlet towards the welding interface. To ensure a fail-safe approach, a relief valve is placed. A flexible hose made of very low thermal conductivity stainless steel (braided type) is attached to the nozzle at one end and the stainless steel pipe at the other end, in order to supply the liquid nitrogen. Careful thermal insulation is done with help of foam (polymer in nature) in order to prevent being affected by external heat during the transfer. The nozzle is availed to point the fluid towards the friction stir welding zone [12, 14–18, 20–22]. An AWM720P1 flow sensor is availed to ensure a constant volume flow rate for liquid nitrogen at 1 bar pressure atmospheric pressure which is 1.977 litres/minute, by taking the total head loss in consideration, elevation point of the FSW setup, and having initial velocity and exit pressure to be zero.

2.2. Tool and Workpiece for Friction Stir Welding. The FSW operation was availed using three types of tools, i.e., involute, step, and thread tool, as indicated in Figure 5.

Each of the friction stir welding tools is distinctive and is availed to enhance the operation of welding in dry and cryogenic conditions. The tool being nonconsumable is the major factor for deciding the temperature differential in the operation. Variable weld speed and pipe speed (workpiece) are chosen based on preliminary experiments [6, 10, 14]. The tool is made of AISI M2 tool steel, whose dimensional details are listed in Figure 5. The tool holds distinctive hardness and is highly resistant to wear properties in correlation to the workpiece taken under consideration.

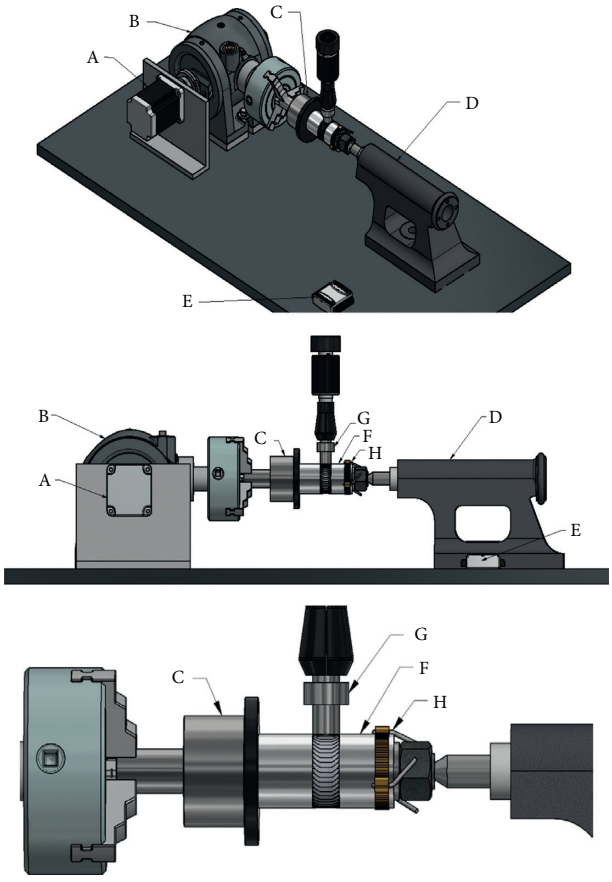

(A) Stepper motor
(B) Driving gear convertor
(C) Developed fixture Assembly
(D) Tail stock
(E) Thermocouple DAQ (Data Acquisition system)
(F) workpiece
(G) Tool
(H) Thermocouple

Figure 1: Friction stir welding components and mechanism of welding.

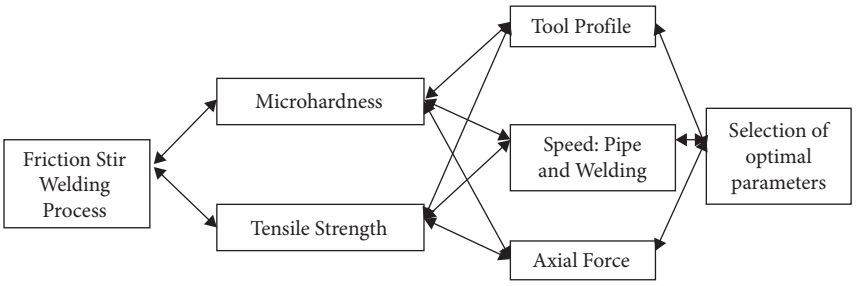

Figure 2: Friction stir welding operation parameters.

The workpiece under consideration is AA 7075 aluminium alloy, whose chemical and physical properties are tabulated in Tables 2 and 3, respectively.

The AA 7075 aluminium alloy constitutes zinc as its major alloying element. Due to its internal resistance to high stress and fatigue strength, also possessing better machinability, it is availed for transport applications in automotive, marine, and aviation firms. Also, these are availed as brazed/welded barrels in defence rifles. Airframes and bicycle frames are made of AA 7075 aluminium alloy, and welding plays a significant role in each of them [3, 4, 7, 11]. The dimensions of the workpiece (pipe tube) for the FSW cycle are depicted in Figure 6, and the workpiece placement is depicted in Figure 7.

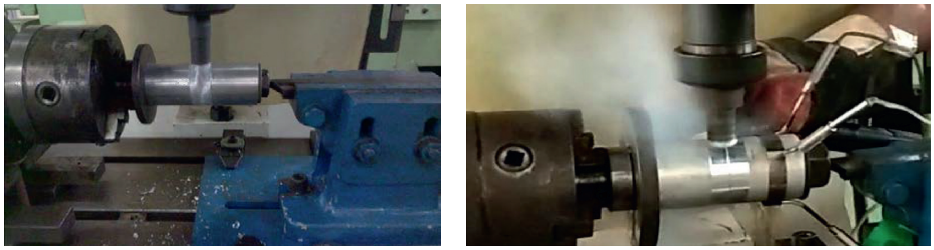

(a) (b)

Figure 3: (a) Dry. (b) Cryogenic- (LN_2-) assisted friction stir welding operation.

Figure 4: Images of the setup.

Table 1: Cryogenic broaching setup components.

S. no.	Components
1.	TA55 liquid nitrogen container
2.	Compressor
3.	Drier
4.	Pressure regulator
5.	Pneumatic hose
6.	Stainless steel pipes
7.	Pressure relief valve
8.	Braided stainless steel hose
9.	Nozzle

2.3. Responses Measurement Methods

2.3.1. Temperature Measurement (Monitoring Perspective). A *K*-type (diameter: 3 mm) thermocouple is availed to measure the temperature and keep a close online monitoring of the temperature around the weld region. The specifications of the same are mentioned in Figure 8 and Table 4.

The concept of novelty exists in the monitoring of temperature values as it is mentioned with a drop in differential without compromising the welding process which

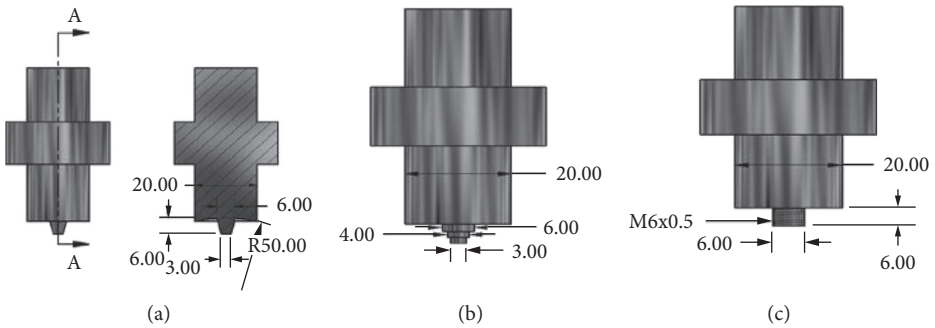

Figure 5: Design of the friction stir welding tool. (a) Involve type (IT). (b) Step type (SS). (c) Thread type (ST).

Table 2: Chemical composition of AA 7075.

Element	Al	Zn	Cr	Ti and Si	Fe	Cu	Mn	Mg
% Nominal	87.1–91.4	5.1–6.1	0.18–0.24	<0.4	<0.5	1.2–2	<0.3	2.1–2.9
% Actual	90.77	5.23	0.24	0.04	0.30	1.13	0.03	2.09

Table 3: Properties of AA 7075 aluminium alloy.

Attributes	Value
Density (kg/m^3)	2810
Tensile strength: ultimate (MPa)	572
Tensile strength: yield (MPa)	503
Modulus of elasticity (GPa)	71.7
Poisson's ratio	0.33
Heat capacity (nature: specific at 100°C) (kJ/kg-K)	0.96
Thermal conductivity (at 100°C) (W/mK)	130
Melting point (°C)	620

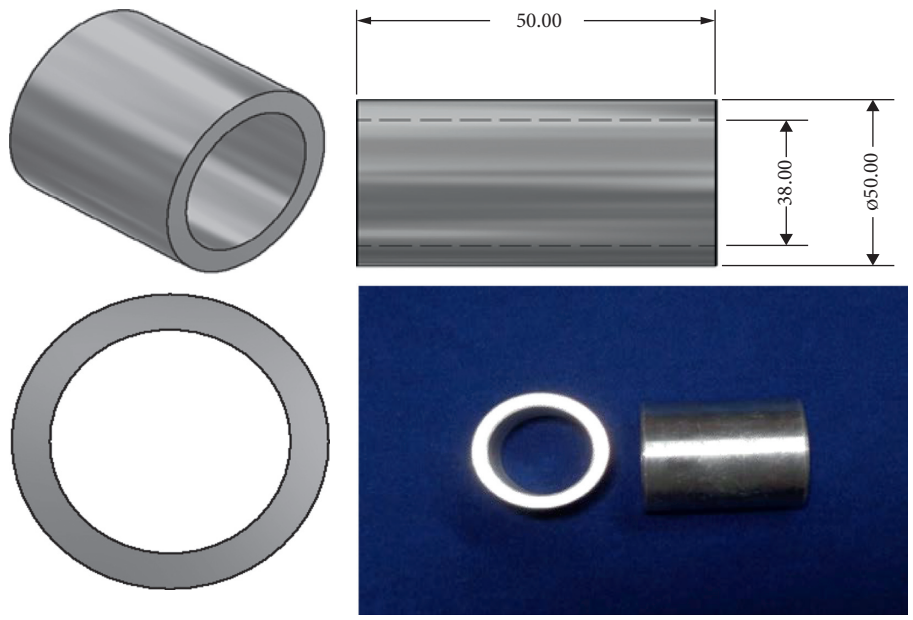

Figure 6: (a) Workpiece draft. (b) FSW (workpiece) component.

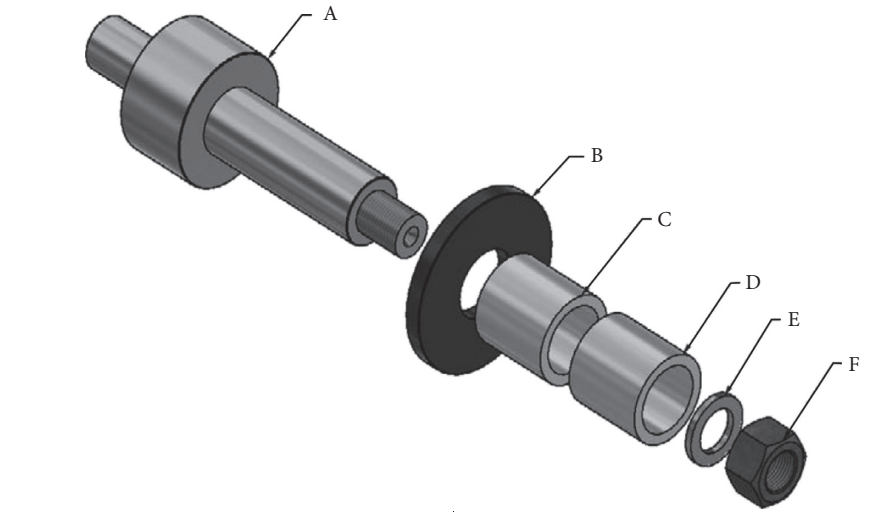

(A) Mandrel (Inner support)
(B) Plate for removing workpiece after weld through hydraulic press
(C) workpiece 1
(D) workpiece 2
(E) washer
(F) Nut

Figure 7: Developed fixture assembly for friction stir welding of AA 7075 aluminium alloys. Developed fixture assembly before and after the FSW process.

(a) (b)

Figure 8: (a) Slots made in the piped tube (workpiece). (b) Placement of *K*-type thermocouple in the FSW setup.

Table 4: *K*-type thermocouple specifications.

Wire leg materials	Chrome-alumel
Sensitivity (μV/°C)	39–43
Temperature range (°C)	−215 to 1310
Resolution (°C)	0.5

improves the efficacy of the parent material to be welded [12, 13, 15, 19]. The temperature was converted using a data acquisition system (DAQ). The range of availing a *K*-type thermocouple is its sensitivity factor being 39–43 μV/°C and thus has a working temperature of −199°C to +1270°C [12, 13, 15].

2.3.2. Microhardness Measurement (Response: Attribute). The microhardness of the friction stir-welded component is significant, as the quality of the operation in disparate environments is dependent on the final strength of the welded material. This is evaluated by Vickers (scale: microns) illustrated in Figure 9, with dead weight loads of 0.01–1 kg and 2 kg options [15].

2.3.3. Tensile Strength (Response: Attribute). Tensile testing specimens were machined according to the dimensions of ASTM standards. Specimens for the tensile test were prepared using a wire electro discharge machine (WEDM) as per ASTM-E8 standard, and the ultimate tensile strength was measured using an electromechanical universal testing machine, as depicted in Figure 10.

2.4. Friction Stir Welding in Disparate Environmental Conditions. For performing friction stir welding of AA 7075 aluminium alloys in the dry and cryogenic environment, orthogonal (L_{27}) array is availed [5, 15, 19, 21–25] after running an in-depth preliminary testing before finalizing on the working range for the input factors. The parameters taken in consideration are microhardness and tensile strength in correlation to tool pin profile, pipe rotation speed, welding speed, and axial force applied on the parent material. The experimental values after conduction of friction stir welding of aluminium alloy are tabulated in Table 5.

Analysing and applying multiattribute algorithms, researchers have established disparate methods of solving the multiple attribute-response problem. The commonly availed technique is ELECTRE, GREY, TOPSIS, and VIKOR [12, 13, 15, 19, 21–25] in which TOPSIS holds a higher ground due to its simplicity in adapting, minimal variation, and drop in complexity with involvement of multiple vectors (provides a common vector plane solution). The method adopted for analyzing the attributes and responses is indicated in Figure 11.

The criteria of importance for factors under consideration are listed out by Simos weighting criteria method which is tabulated in Table 6 [19].

The valuation obtained using the TOPSIS method is listed out in Tables 7 and 8 for dry and cryogenic friction stir welding, respectively.

From the criteria analysis (preference to unity factor), tool profile stepped type, pipe rotation speed of 1000 rpm, welding speed of 50 mm/min, and axial force of 8 kN are close to unity, i.e., ideal solution for dry and cryogenic friction stir welding of AA 7075 aluminium alloys [12, 15, 19, 22–25]. These close to ideal samples are taken to study the individual microstructural properties affecting the welding zone in disparate environmental conditions.

3. Results and Discussion

3.1. Effect of Responses on Factors of Friction Stir Welding. An increase of 0.76–42.93% and 3.79–31.24% in microhardness and tensile strength, respectively, is ascertained in cryogenic friction stir welding in correlation to dry friction stir welding of aluminium alloys, which is tabulated in Table 9 and depicted in Figure 12.

Figure 9: Microhardness tester.

3.2. Ramification of Microhardness in FSW of Aluminium Alloy. The hardness test was conducted on 27 specimens for disparate friction stir-welded conditions for AA 7075 aluminium alloy, as depicted in Figure 13. For a clear understanding, the micro-Vickers hardness test was conducted on different zones of the welded material, as depicted in Figure 13, and corresponding values are tabulated in Table 10.

The important zones are parent zone, heat affected zone (HAZ), and weld zone. From the analysis, it was found that the heat affected zone showcases the least hardness value as maximum heat is absorbed in this region creating the coarse and fine granular irregular structure. From Table 10, we can observe an increment of 42.05%, 11.11%, and 14.73% in the hardness value for the cryogenic FSW process for AA 7075 aluminium alloys in correlation to the dry FSW process in HAZ, TMZ, and NZ areas. The hardness values were obtained at 1.5 mm below the weld surface [11]. The presence of precipitates of magnesium and zinc ($MgZn_2$) leads to the curtailing of the hardness in the FSW process [2, 3].

Excessive temperature differential occurring in the dry FSW process leads to metastable precipitates that cause a drop in the hardness in the weld region [3, 4, 10]. An immediate remedy is found in the cryogenic FSW process due to the fine structures occurring in the region, thus creating a brittle transition region along the weld area [5]. In the cryogenic FSW process, the dissolved precipitates are curtailed due to the drop in temperature differential [12, 13, 15].

3.3. Ramification of Tensile Strength in FSW of Aluminium Alloy. The tensile samples taken for consideration are depicted in Figure 14, and the tensile properties are dependent on the microstructure and friction stir welding environment. The tensile plot for the friction stir-welded joints for the dry and cryogenic condition for AA 7075 alloy is shown in Figure 15.

A steady tensile strength is ascertained in the cryogenic condition owing to fine precipitate formation, which gets distributed in a fine homogeneous pattern having a definite

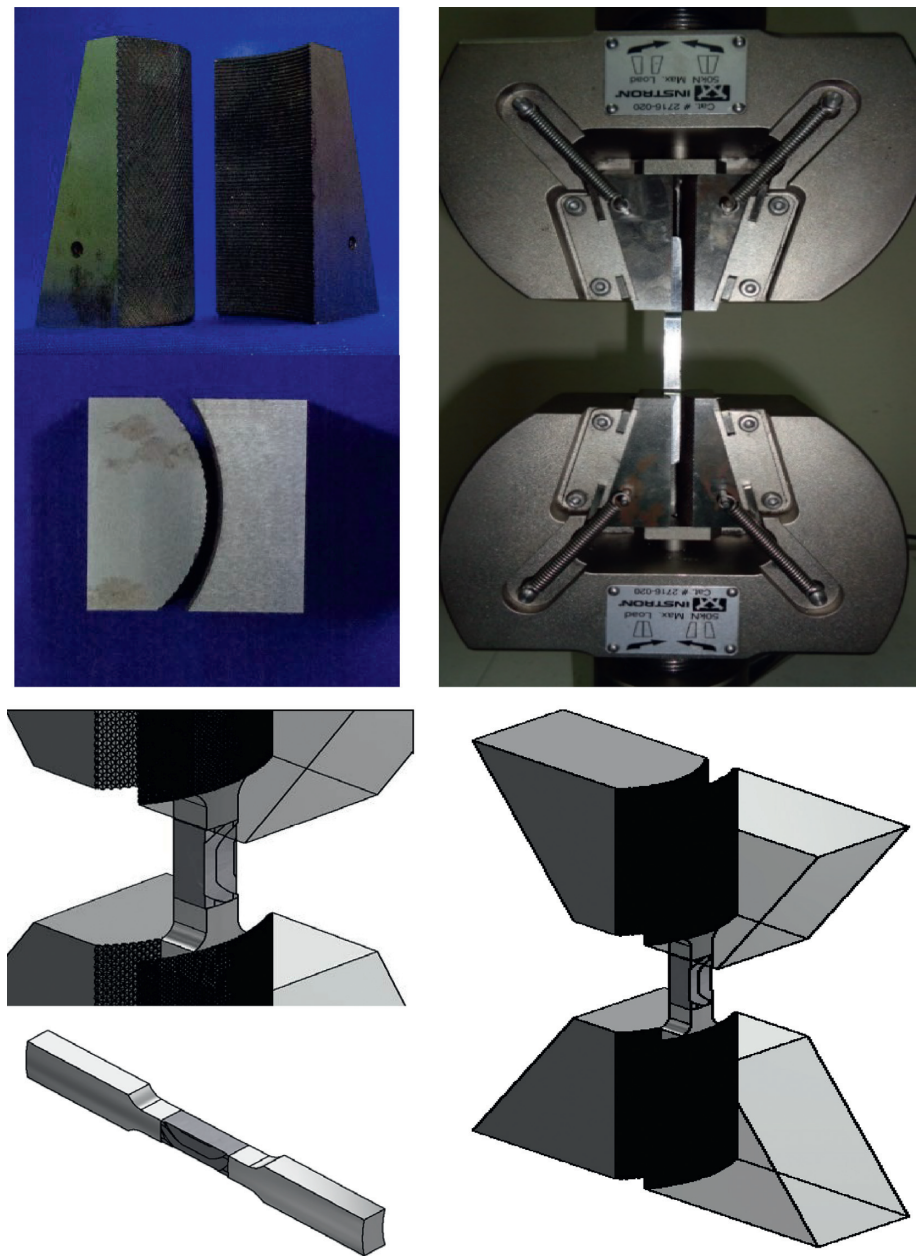

Figure 10: Universal testing machine and friction stir-welded AA 7075 aluminium alloy.

Table 5: Orthogonal array experiment (L_{27}) for dry and cryogenic friction stir welding of AA 7075 aluminium alloy.

S. no.	Tool pin profile (m/min)	Pipe rotation speed (rpm)	Welding speed (mm/min)	Axial force (kN)	Microhardness HV		Tensile strength (MPa)	
					Dry	LN_2	Dry	LN_2
1	SS	1000	50	8	100.2	164.334	164.334	168.582
2	SS	1000	50	8	90.2	164.7	164.7	167.931
3	SS	1000	50	8	100.1	146.05	146.05	166.56
4	SS	1100	60	10	99.3	160.049	160.049	165.487
5	SS	1100	60	10	89.5	151.025	151.025	170.68
6	SS	1100	60	10	97.5	166.042	166.042	161.1015

Table 5: Continued.

S. no.	Tool pin profile (m/min)	Pipe rotation speed (rpm)	Welding speed (mm/min)	Axial force (kN)	Microhardness HV		Tensile strength (MPa)	
					Dry	LN_2	Dry	LN_2
7	SS	1200	70	12	97.6	171.178	171.178	167.372
8	SS	1200	70	12	85.3	161.911	161.911	176.85
9	SS	1200	70	12	95.3	162.027	162.027	171.276
10	ST	1000	60	12	101.2	84.412	84.412	120.653
11	ST	1000	60	12	113.4	113.284	113.284	123.873
12	ST	1000	60	12	100.2	121.927	121.927	120.998
13	ST	1100	70	8	97.8	134.026	134.026	146.285
14	ST	1100	70	8	111.5	132.751	132.751	141.002
15	ST	1100	70	8	97.6	124.287	124.287	143.056
16	ST	1200	50	10	95.7	115.88	115.88	99.461
17	ST	1200	50	10	105.3	75.563	75.563	98.329
18	ST	1200	50	10	95.3	83.681	83.681	118.277
19	IT	1000	70	10	94.1	117.797	117.797	135.678
20	IT	1000	70	10	99.1	44.672	44.672	139.523
21	IT	1000	70	10	101.6	134.052	134.052	139.081
22	IT	1100	50	12	91.8	138.651	138.651	150.522
23	IT	1100	50	12	97.5	148.456	148.456	153.886
24	IT	1100	50	12	98.6	130.76	130.76	155.721
25	IT	1200	60	8	90.3	140.881	140.881	152.027
26	IT	1200	60	8	93.7	121.963	121.963	141.658
27	IT	1200	60	8	95.7	115.959	115.959	135.216

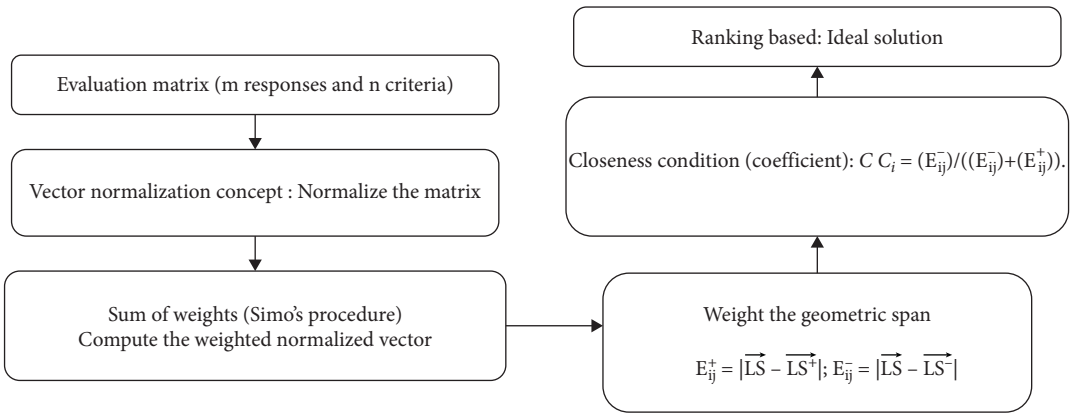

Figure 11: Methodology of TOPSIS (close to ideal solution).

Table 6: Computational steps of Simos weighting procedure.

Subset criteria	Number of criteria (variables)	Number of position	Nonnormalized weighted matrix	Total (%)
Microhardness	1	1	1/2*100 = 50–50	50
Tensile strength	1	1	1/2*100 = 50–50	50

boundary (grain) condition [5]. The strengthening of these alloys is attributed to the metastable phase formed in cryogenic friction stir welding [3, 7]. The coarse structures, ascertained in dry friction stir welding, create a drop in the tensile strength [6–8].

3.4. Microstructure Study. The friction stir-welded condition is analyzed to understand the surface of AA 7075 aluminium alloy, with a magnification of 25x availed in a optical microscope to determine the microstructure of the welded component, as indicated in Figure 16.

Table 7: TOPSIS evaluation for dry friction stir welding of AISI 4340 steel.

S. no.	Tool pin profile (m/min)	Pipe rotation speed (rpm)	Welding speed (mm/min)	Axial force (kN)	Weighted		Distance from ideal solution		CC	Rank
					WH	WT	E_{ij}^{+}	E_{ij}^{-}	CC_{ij}	
1	SS	1000	50	8	0.10	0.12	0.01	0.09	0.86	1
2	SS	1000	50	8	0.09	0.12	0.02	0.09	0.79	6
3	SS	1000	50	8	0.10	0.10	0.02	0.07	0.77	8
4	SS	1100	60	10	0.10	0.11	0.02	0.08	0.84	4
5	SS	1100	60	10	0.09	0.11	0.03	0.08	0.73	10
6	SS	1100	60	10	0.10	0.12	0.02	0.09	0.85	3
7	SS	1200	70	12	0.10	0.12	0.02	0.09	0.85	2
8	SS	1200	70	12	0.08	0.12	0.03	0.08	0.75	9
9	SS	1200	70	12	0.09	0.12	0.02	0.08	0.82	5
10	ST	1000	60	12	0.10	0.06	0.06	0.03	0.34	24
11	ST	1000	60	12	0.11	0.08	0.04	0.06	0.58	20
12	ST	1000	60	12	0.10	0.09	0.04	0.06	0.60	18
13	ST	1100	70	8	0.10	0.10	0.03	0.07	0.68	15
14	ST	1100	70	8	0.11	0.10	0.03	0.07	0.71	11
15	ST	1100	70	8	0.10	0.09	0.04	0.06	0.61	17
16	ST	1200	50	10	0.09	0.08	0.04	0.05	0.55	23
17	ST	1200	50	10	0.10	0.05	0.07	0.03	0.30	26
18	ST	1200	50	10	0.09	0.06	0.07	0.03	0.31	25
19	IT	1000	70	10	0.09	0.08	0.04	0.05	0.55	21
20	IT	1000	70	10	0.10	0.03	0.09	0.01	0.13	27
21	IT	1000	70	10	0.10	0.10	0.03	0.07	0.69	12
22	IT	1100	50	12	0.09	0.10	0.03	0.07	0.68	14
23	IT	1100	50	12	0.10	0.11	0.02	0.08	0.77	7
24	IT	1100	50	12	0.10	0.09	0.03	0.06	0.66	16
25	IT	1200	60	8	0.09	0.10	0.03	0.07	0.69	13
26	IT	1200	60	8	0.09	0.09	0.04	0.06	0.58	19
27	IT	1200	60	8	0.09	0.08	0.04	0.05	0.55	22

Table 8: TOPSIS evaluation for cryogenic friction stir welding of AISI 4340 steel.

S. no.	Tool pin profile m/min	Pipe rotation speed (rpm)	Welding speed (mm/min)	Axial force (kN)	Weighted		Distance from ideal solution		CC	Rank
					WH	WT	E_{ij}^{+}	E_{ij}^{-}	CC_{ij}	
1	SS	1000	50	8	0.10	0.11	0.01	0.05	0.87	1
2	SS	1000	50	8	0.09	0.11	0.01	0.05	0.77	3
3	SS	1000	50	8	0.10	0.11	0.01	0.05	0.81	2
4	SS	1100	60	10	0.09	0.11	0.01	0.04	0.76	4
5	SS	1100	60	10	0.09	0.11	0.02	0.05	0.73	6
6	SS	1100	60	10	0.09	0.11	0.02	0.04	0.67	11
7	SS	1200	70	12	0.09	0.11	0.02	0.05	0.67	10
8	SS	1200	70	12	0.09	0.12	0.02	0.05	0.73	7
9	SS	1200	70	12	0.09	0.11	0.02	0.05	0.73	8
10	ST	1000	60	12	0.10	0.08	0.04	0.02	0.39	23
11	ST	1000	60	12	0.10	0.08	0.03	0.02	0.40	22
12	ST	1000	60	12	0.10	0.08	0.04	0.02	0.36	24
13	ST	1100	70	8	0.09	0.10	0.02	0.03	0.57	16
14	ST	1100	70	8	0.11	0.09	0.02	0.03	0.60	14
15	ST	1100	70	8	0.10	0.09	0.02	0.03	0.60	15
16	ST	1200	50	10	0.10	0.07	0.05	0.01	0.17	27
17	ST	1200	50	10	0.10	0.06	0.05	0.01	0.21	26
18	ST	1200	50	10	0.09	0.08	0.04	0.01	0.25	25

Table 8: Continued.

S. no.	Tool pin profile m/min	Pipe rotation speed (rpm)	Welding speed (mm/min)	Axial force (kN)	Weighted		Distance from ideal solution		CC	Rank
					WH	WT	E_{ij}^{+}	E_{ij}^{-}	CC_{ij}	
19	IT	1000	70	10	0.10	0.09	0.03	0.03	0.53	19
20	IT	1000	70	10	0.10	0.09	0.02	0.03	0.56	17
21	IT	1000	70	10	0.10	0.09	0.03	0.03	0.54	18
22	IT	1100	50	12	0.10	0.10	0.02	0.04	0.66	12
23	IT	1100	50	12	0.10	0.10	0.02	0.04	0.68	9
24	IT	1100	50	12	0.10	0.10	0.01	0.04	0.74	5
25	IT	1200	60	8	0.09	0.10	0.02	0.04	0.60	13
26	IT	1200	60	8	0.09	0.09	0.03	0.03	0.50	20
27	IT	1200	60	8	0.09	0.09	0.03	0.03	0.45	21

Table 9: Effect of cryogenic over dry friction stir welding for AA 7075 aluminium alloys.

S. no.	Tool pin profile (m/min)	Pipe rotation speed (rpm)	Welding speed (mm/min)	Axial force (kN)	% increase in microhardness in cryogenic FSW	% increase in tensile strength in cryogenic FSW
1	SS	1000	50	8	2.58	20.16
2	SS	1000	50	8	1.96	23.95
3	SS	1000	50	8	14.04	16.08
4	SS	1100	60	10	3.40	12.99
5	SS	1100	60	10	13.01	18.88
6	SS	1100	60	10	2.98	8.51
7	SS	1200	70	12	2.22	3.79
8	SS	1200	70	12	9.23	21.45
9	SS	1200	70	12	5.71	10.49
10	ST	1000	60	12	42.93	21.74
11	ST	1000	60	12	9.35	6.97
12	ST	1000	60	12	0.76	18.26
13	ST	1100	70	8	9.15	12.99
14	ST	1100	70	8	6.22	13.18
15	ST	1100	70	8	15.10	23.46
16	ST	1200	50	10	14.17	18.60
17	ST	1200	50	10	30.13	11.40
18	ST	1200	50	10	41.34	12.59
19	IT	1000	70	10	15.18	31.24
20	IT	1000	70	10	212.33	22.70
21	IT	1000	70	10	3.75	16.34
22	IT	1100	50	12	8.56	27.78
23	IT	1100	50	12	3.66	18.15
24	IT	1100	50	12	19.09	22.21
25	IT	1200	60	8	7.91	17.28
26	IT	1200	60	8	16.15	13.34
27	IT	1200	60	8	16.61	15.15

The need for microstructure analysis is important as this indicates the hardness, strength, and corrosion resistance of the welded surface as these form the crux for applications in the industrial perspective [15, 19]. Detailed microstructure analysis and SEM images are shown in Figure 17–20 for dry and cryogenic FSW of AA 7075 aluminium alloy.

Friction stir-welded aluminium alloy consists of precipitates in the form magnesium zinc ($MgZn_2$) which are predominant in dry condition welding, as the materials' grain size in original that was observed was 92 microns before the friction stir welding process was carried out in two different mediums [6]. A decrement of 21.68% is observed in the grain size in the cryogenic condition in correlation to the dry FSW process, indicating a drop in the coarse structure, as tabulated in Table 11 [7, 12–15].

In the cryogenic condition, equiaxed and fine grains are ascertained in the weld zone, which indicates a drop in the grain size owing to smaller intermetallics formed in the zone of welding [12]. With a drop in temperature in the cryogenic condition, a continuous evaporation pad is formed which removes the temperature differential occurring at the zone of welding [12–14, 19]. The presence of wide craters/microvoids

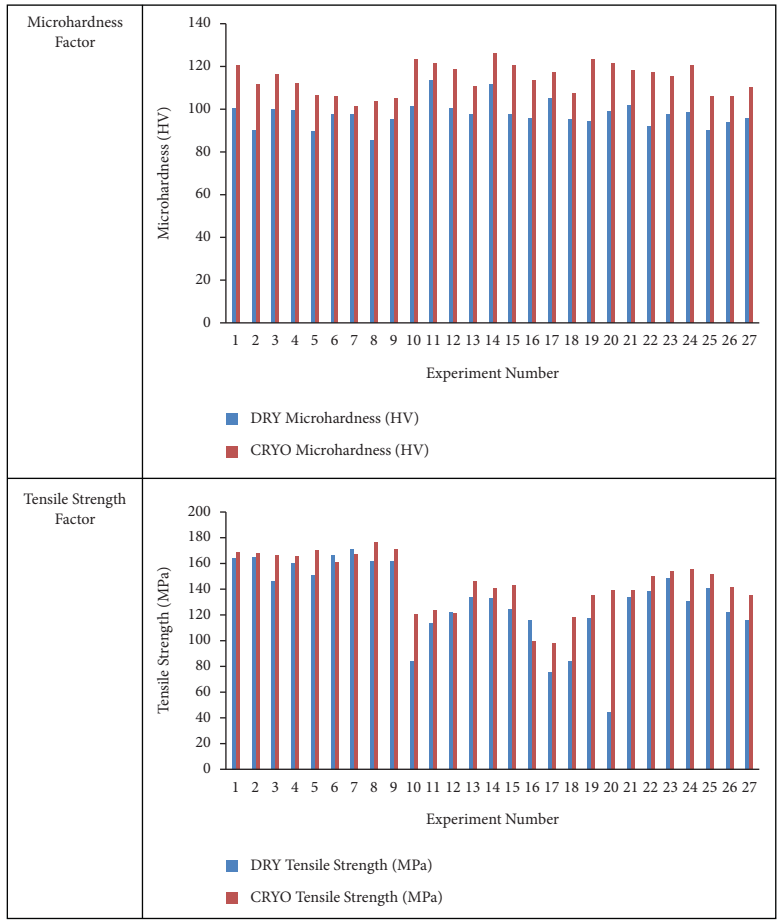

Figure 12: Comparison study of dry and cryogenic friction stir welding of AA 7075 aluminium alloys.

A AA 7075 Pipe 1
B AA 7075 Pipe 2
1 Parent Area
2 Heat affected zone
3 Weld interface
4 Weld area

(a)

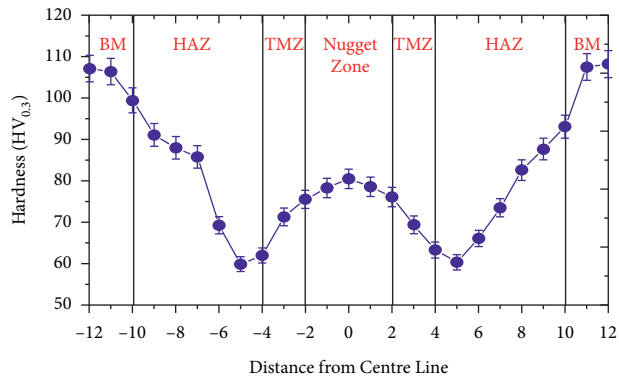

BM Base Material
HAZ Heat affected zone
TMZ Thermo Mechanically Affected Zone
NZ Nugget zone

(b)

Figure 13: Continued.

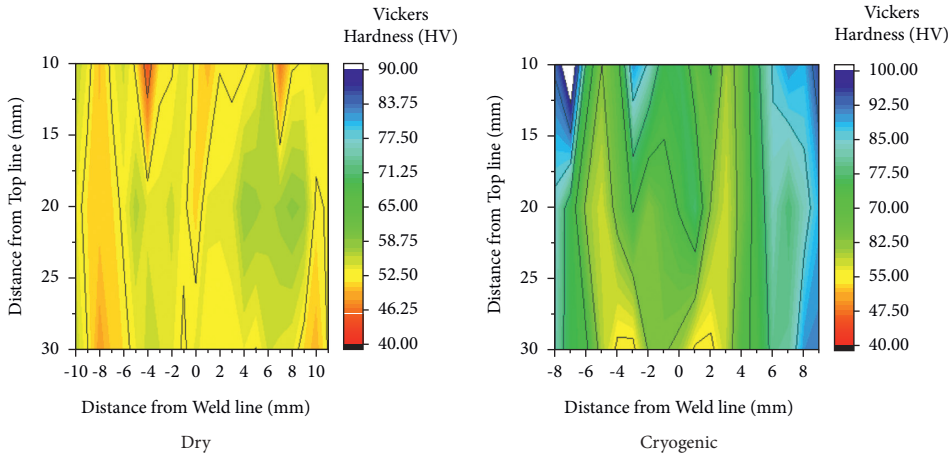

(c)

Figure 13: (a) Macroimage showing disparate regions of FSW AA 7075 alloy. (b) Hardness measurement of depicting disparate regions of FSW AA 7075 alloy. (c) Hardness survey for the weld region for FSW AA 7075 alloy.

Table 10: Micro-Vickers hardness value for different zones of friction stir-welded AA 7075 alloys (a sample chosen for the disparate region).

Zone	Zone name	Dry	Cryogenic
1	Base material	122	122
2	Heat affected zone	62	107
3	Thermo-mechanically affected zone	72	81
4	Nugget zone	81	95

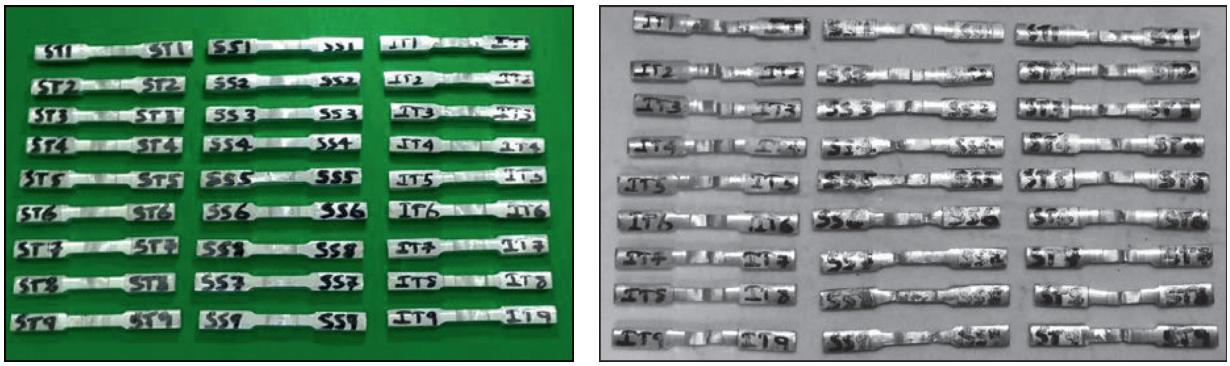

(a) (b)

Figure 14: FSW specimens taken (a) before and (b) after the tensile test.

is substantially present in dry condition welding due to the colossal temperature differential and increased friction factor (nonavailability of lubrication) [18]. Additionally, the component of hard residual factor and flowability (stress) on the workpiece is substantial when it comes to welding. With a drop in temperature differential, cryogenic friction stir welding causes an indirect curtailment of flow stress and drop in the tensile factor (residual) [5, 22]. The rough coarse grains in dry FSW is owing to the precipitate formation (intermetallic fusion) [2]. Also, having induced stresses along the line of weld causes colossal surface roughness leading to uneven and irregular distribution of the material along the welded region. An abatement of microcraters and fine-grain structures is obtained in the cryogenic friction stir-welded condition owing to the homogeneity of the welding process in correlation to the dry FSW process for AA 7075 aluminium alloy [22, 25]. Dry FSW induces the tensile residual factor in AA 7075 alloy, which leads to attenuation of microcracks leaving short of applications in the area of high stress loading conditions [6, 15].

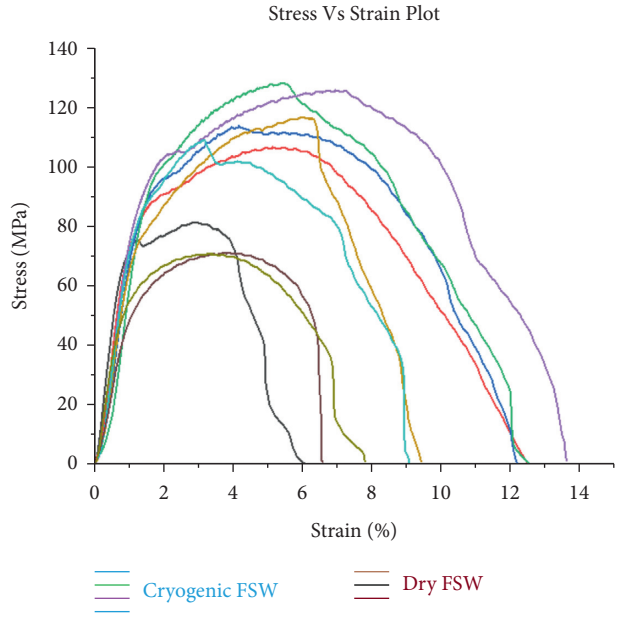

Figure 15: Stress-strain diagram, for the friction stir-welded sample in the dry and cryogenic condition for AA 7075 aluminium alloy.

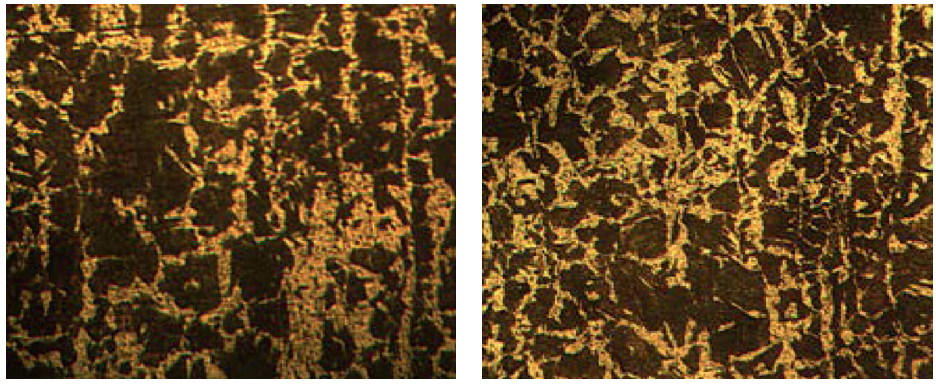

(a) (b)

Figure 16: Friction stir welding samples under (a) dry and (b) cryogenic condition.

3.5. AFM Analysis. The study of the surface (topographical) is carried out by atomic force microscopy (AFM) for dry and cryogenic friction stir welding of AA 7075 aluminium alloy. The profile image is depicted in Figure 21, whose profile (average) roughness is tabulated in Table 12.

From the microstructure study, high craters were observed in dry friction stir welding, and also from Figure 21, extensive waviness pattern is ascertained indicating the irregular weld zone (HAZ) due to presence of coarse grains [5, 6, 19, 24, 25].

A curtailment of 50.84% is ascertained in the roughness value in cryogenic friction stir welding in correlation to dry friction stir welding of AA 7075 alloy. The surface roughness decrease can be attributed to the curtailment of the HAZ zone, as decrease in the roughness parameter is dependent on the temperature differential drop (lower amount of heat conducted to the HAZ zone) [24]. Also, a drop in the surface roughness factor indicates grain refinement occurring in the welding surface [11, 19]. Along with a drop in temperature differential, curtailment of surface roughness results in higher grain refinement, as ascertained in the cryogenic friction stir welding condition. The waviness pattern is ascertained in both the welding conditions due to the irregularity in the surface (disorientation of grains). The analysis (topographical) plays a key role in analyzing the boundary edges, corrosion phenomenon, and residual factor (compressive stress) [5, 23].

3.6. XRD Analysis. The residual factor (stress) plays a key role in applications of welding. A welded material undergoes high compressive and tensile loading at the point of the welding area. The residual factor is calculated by availing sin square technique [13, 22]. While performing the friction stir welding, induced stresses occur due to axial force and

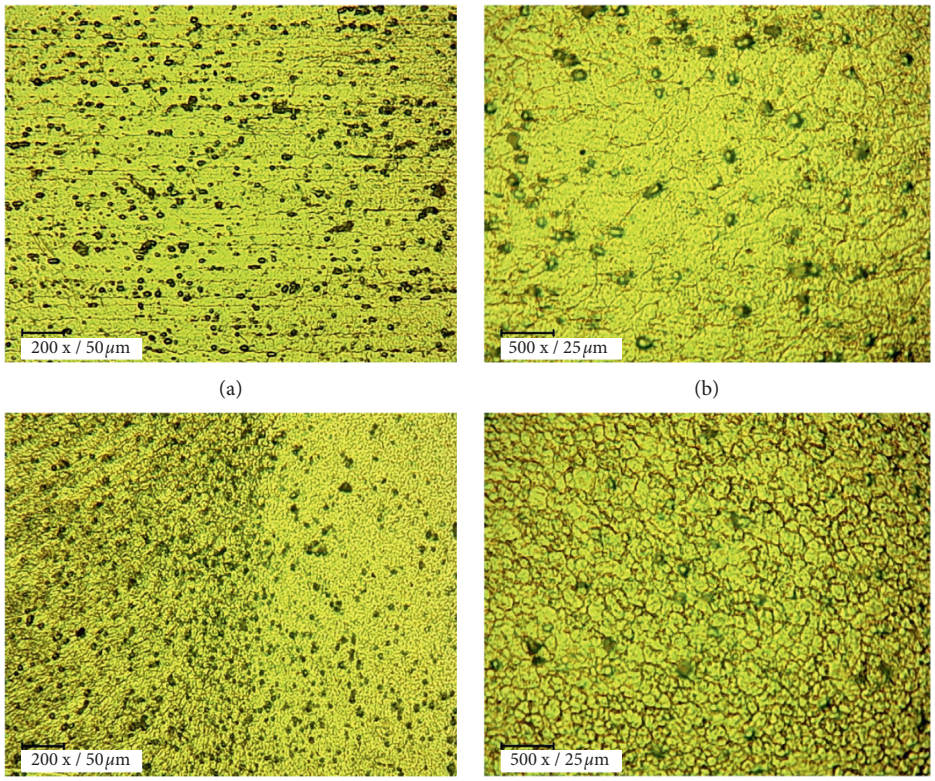

Figure 17: Detailed microscopic image for dry friction stir welding of AA 7075 aluminium alloy. (a) Parent. (b) HAZ. (c) Interface. (d) Weld nugget zone.

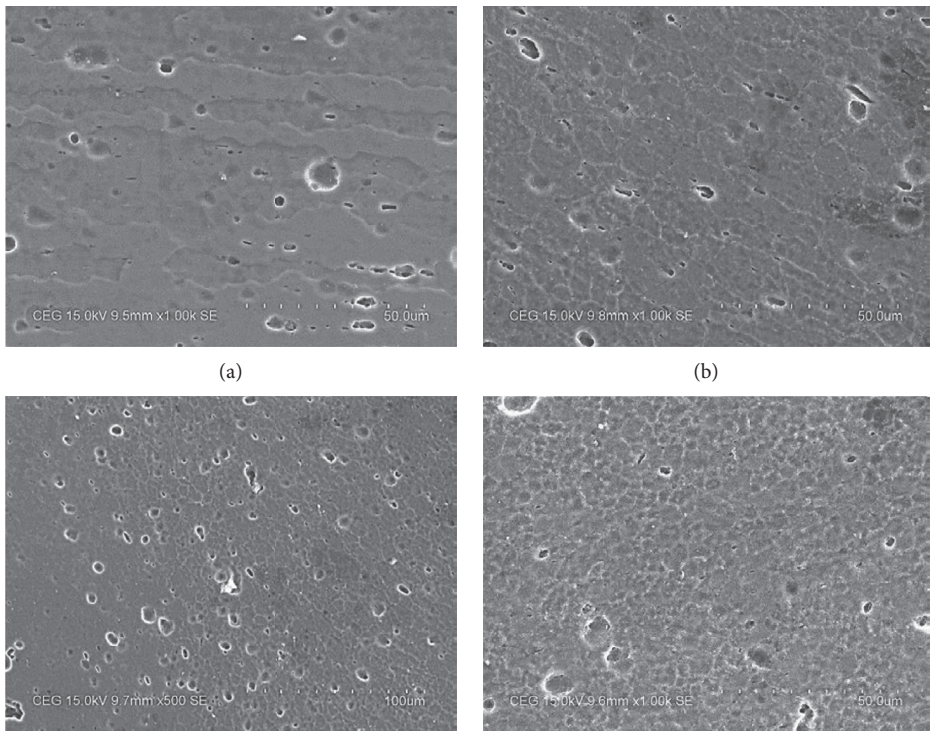

Figure 18: Detailed scanning electron microscopic image for dry friction stir welding of AA 7075 aluminium alloy. (a) Parent. (b) HAZ. (c) Interface. (d) Weld nugget zone.

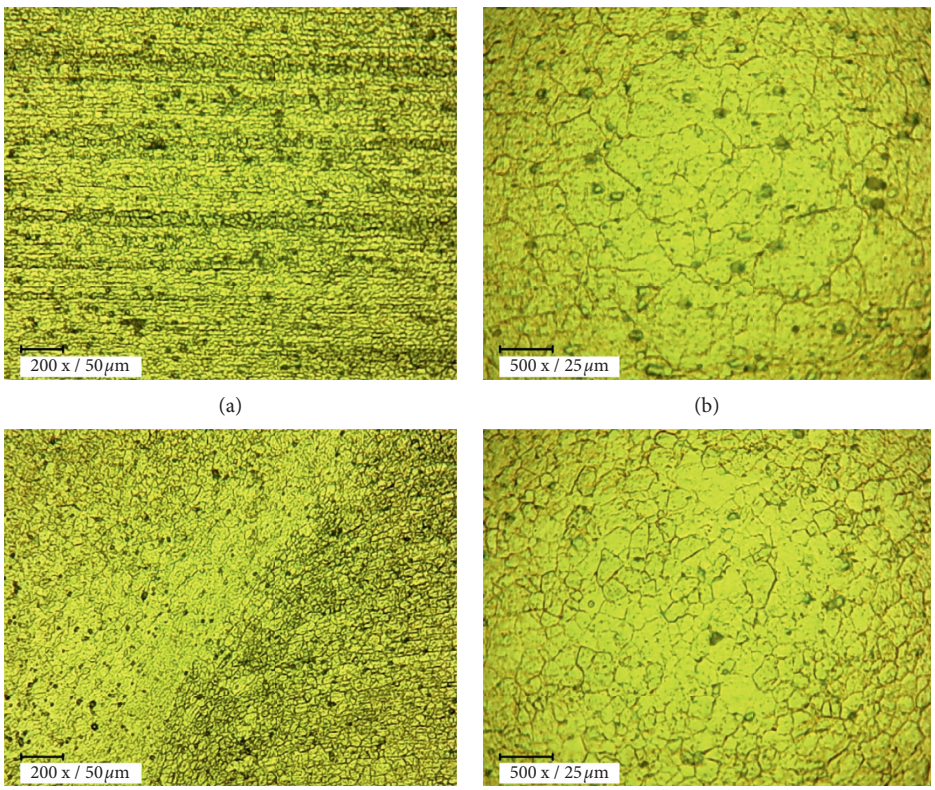

Figure 19: Detailed microscopic image for cryogenic friction stir welding of AA 7075 aluminium alloy. (a) Parent. (b) HAZ. (c) Interface. (d) Weld nugget zone.

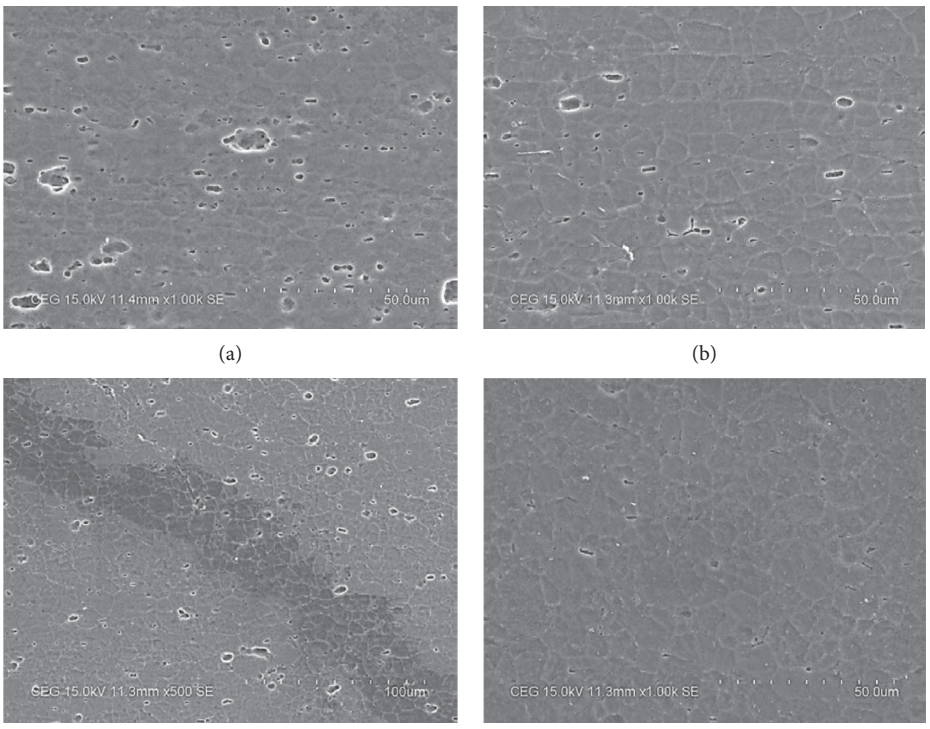

Figure 20: Detailed scanning electron microscopic image for cryogenic friction stir welding of AA 7075 aluminium alloy. (a) Parent. (b) HAZ. (c) Interface. (d) Weld nugget zone.

Table 11: Average grain size of the best and worst sample (using "image J" software).

S. no.	Microstructure condition	Average grain size (μ)
1	Dry FSW condition	60.17
2	Cryogenic FSW condition	47.12

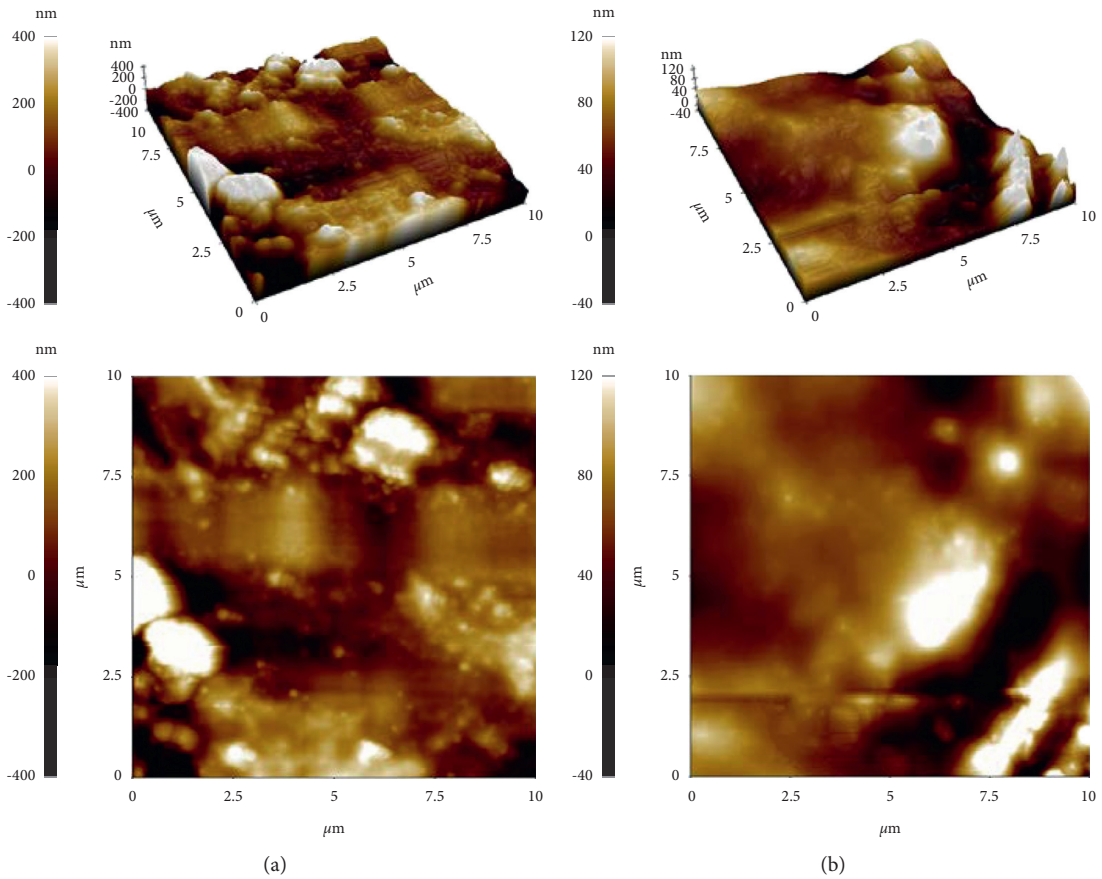

Figure 21: Atomic force microscopy of (a) dry and (b) cryogenic friction stir-welded AA 7075 samples.

Table 12: Topographical analysis of AISI 4340 in dry and cryogenic friction stir welding surfaces.

Broaching	Roughness factor (nm)
Dry	238
Cryogenic	117

Table 13: Residual stress (compressive) analysis of AA 7075 friction stir-welded samples.

Residual stress values (MPa)	Dry	Cryogenic
	89.14	148.93

temperature differential (colossal) occurring in disparate regions of the welding material, which plays a key role in determining the surface attributes of the operation [3, 25]. The factor of stress is tabulated in Table 13, and the correlated XRD plots are depicted in Figure 22 and further analyzed availing $\sin^2\psi$ technique [5, 12].

From the analysis, it is found that the compressive residual factor increases by 40.14% in cryogenic friction stir welding in correlation to dry friction stir welding of AA7075 aluminium alloy. The attenuation in the residual factor indicates higher weld life integrity manufactured under cryogenic conditions. In the XRD plot, a shift in the peak is ascertained in the cryogenic friction stir welding condition, indicating higher refinement, a reduction in grain boundaries, thus inducing colossal amount of internal stress in the weld region [4, 8, 23].

The refinement indicates a drop in the grain (average) size along the weld area surface. With a compressive factor, an increase in wear resistance is ascertained along the region. Broadening of peak is ascertained in cryogenic friction stir welding, enhancing the component of strain (lateral factor) along with curtailed dislocations occurring in the weld region due to the subzero welding condition (drop in differential: brittle transition, leaving smaller microstrains devoid of microcracks, and reduction of wear). Width of XRD peak shifts by 39%, indicating a curtailed grain (average) size. These microstrains, dislocations, and drop in

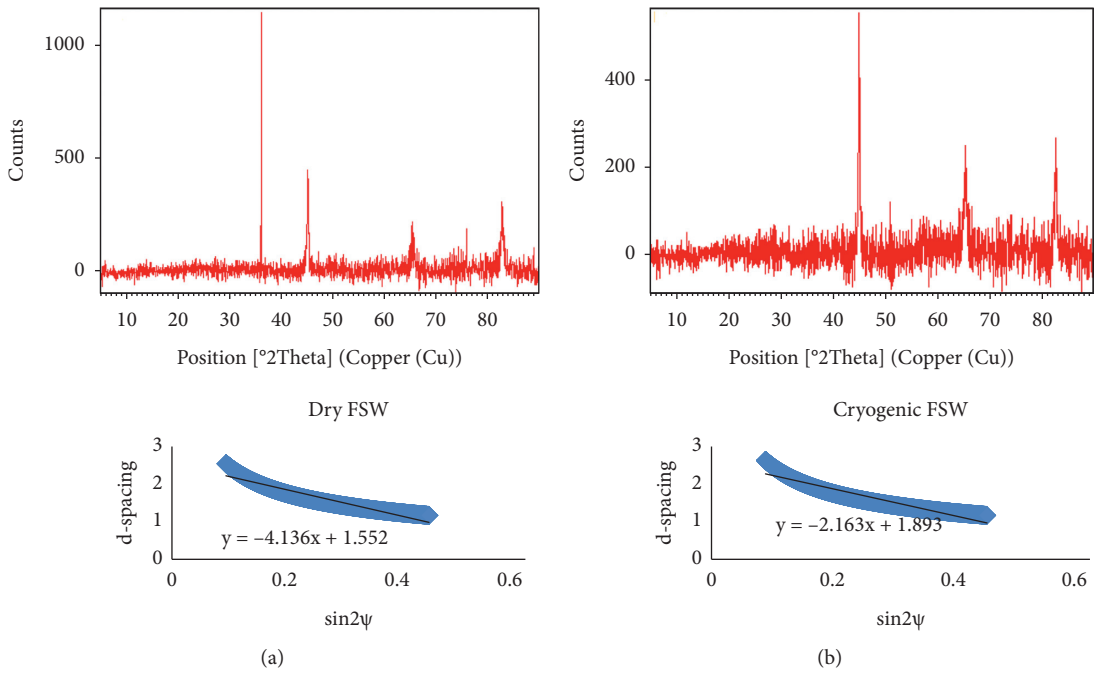

Figure 22: XRD image of (a) dry and (b) cryogenic friction stir-welded AA 7075 aluminium alloys.

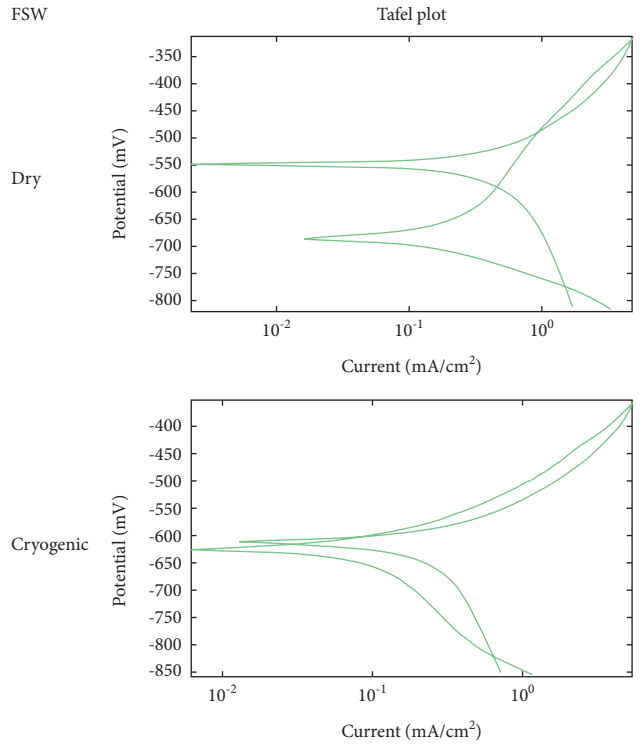

Figure 23: Corrosion analysis for dry and cryogenic friction stir welding of AA 7075 aluminium alloys.

Table 14: Corrosion data recording for dry and cryogenic friction stir welding of AA 7075 aluminium alloys.

FSW	Dry		Cryogenic
Data points	689		692
Rest potential (mV)	−457.39		−477.13
LPR (polarization resistance)	132.47		177.18
I_{corr} (mA/cm^2)	0.6189		0.4051
Corrosion rate (mm/year)	3.894		1.247
Start potential (mV)		−250	
End potential (mV)		250	
Sweep rate (mV/min)		100	
Cycles		1	
B_a (mV)		120	
B_c (mV)		120	

surface roughness bring the factor of corrosion resistance for the welded material under the cryogenic condition [15, 22, 24].

3.7. Corrosion Analysis. A oxidation factor is expected for Al-Al welded joints. In dry FSW of aluminium alloy, frictional heat generation and humidity (atmospheric) of 55% speed up the oxidation rates of aluminium during the welding cycle [6, 19]. The formation of intermetallic compounds consisting of carbon increases the surface roughness factor and induced tensile stresses, thus curtailing the corrosion resistance factor in the dry FSW condition [6]. This phenomenon is devoid in the cryogenic FSW process as the absence of microcracks and void-related problems in the welded region aids in the corrosion resistance factor [6, 8]. A component of weld undergoes extensive cycles of friction, wear, tear, and load factor. The worn out material exposed to environmental conditions in the areas of oil transportation and automotive parts undergoes corrosion with exposure to disparate fluids or air-based application [6, 13, 22, 24]. The anodic polarization changes in the surface of the friction stir-welded component are depicted in Figure 23, and the corresponding corrosion rate is tabulated in Table 14.

The rate of corrosion resistance aggregates by 67.97% in cryogenic FSW in correlation to dry FSW of aluminium alloys, owing to reduction in surface roughness factor, drop in grain size, and surge in the compressive residual factor [6, 14]. When all of these occur in the weld region, an attribute of the passive barrier occurs in the cryo FSW component, indicating higher resistance to corrosion [22, 24]. Presence of secondary phases, indicating grain boundary precipitates, enhances the factor of corrosion resistance and mechanical strength of the welded region, aiding in retainment and augmentation of the barrier (passive region) formed [8, 15].

4. Conclusions

Friction stir welding operation was adopted for joining AA 7075 aluminium alloy (application: oil industries, chemical pipe transportation, and defence barrels) in dry and cryogenic environmental conditions. The major findings of the experimental investigation are

(1) An increase of 0.76–42.93%, and 3.79–31.24% in microhardness and tensile strength, respectively, is ascertained in cryogenic friction stir welding in correlation to dry friction stir welding of aluminium AA7075 alloys.

(2) From the criteria analysis (TOPSIS: preference to unity factor), tool profile stepped type, pipe rotation speed of 1000 rpm, welding speed of 50 mm/min, and axial force of 8 kN are close to unity ideal solution for dry and cryogenic friction stir welding of AA 7075 aluminium alloys.

(3) In cryogenic friction stir welding, a drop in temperature differential is experienced which aids in the curtailment of welding temperature, thereby reducing the internal stresses (tensile) induced on the components surface. These factors alleviate surface morphology by curtailing the coarse structures (precipitates in the form magnesium zinc ($MgZn_2$)) formed in the dry FSW condition, and a decrement of 21.68% is observed in the grain size in the cryogenic condition in correlation to the dry FSW process.

(4) The friction stir-welded component under the cryogenic environment showcased drop in temperature, curtailed surface roughness, and fine grain structure owing to reduction in temperature differential occurring at the weld zone. A curtailment of 50.84% is ascertained in the roughness value in cryogenic friction stir welding in correlation to dry friction stir welding of AA 7075 alloy.

(5) The compressive residual factor increases by 40.14% in cryogenic friction stir welding in correlation to dry friction stir welding of AA7075 aluminium alloy. The attenuation in the residual factor indicates higher weld life integrity manufactured under cryogenic conditions, owing to higher refinement of grain size and a reduction in the grain boundary phenomenon.

(6) Width of XRD peak shifts by 39%, and broadening of peak indicates a curtailed grain (average) size. These microstrains, reduction in dislocations, and drop in surface roughness bring the factor of passivation barrier, aiding in corrosion resistance and high internal stresses opposing the wear component.

(7) The rate of corrosion resistance aggregates by 67.97% in cryogenic FSW in correlation to dry FSW of aluminium alloys, owing to reduction in temperature differential, surface roughness factor, drop in grain size, and surge in the compressive residual factor.

Data Availability

The data used to support the findings of this study are included within the article.

Conflicts of Interest

The authors declare that they have no conflicts of interest.

Acknowledgments

The authors would like to express their sincere thanks to the Council of Scientific and Industrial Research (CSIR), Government of India, New Delhi, for providing the research fund under the scheme of Senior Research Fellowship (Grant no. 09/468/0496/2016 EMRI-I) from April 2017.

References

[1] W. Li, A. Vairis, and R. Mark Ward, "Advances in friction welding," *Advances in Materials Science and Engineering*, vol. 2014, Article ID 204515, 1 page, 2014.

[2] S. Sadiq Aziz, R. Thiru, and A. S. M. T. Izamshah, "Unstable temperature distribution in friction stir welding," *Advances in Materials Science and Engineering*, vol. 2014, Article ID 980636, 8 pages, 2014.

[3] M. Jabbari, "Effect of the preheating temperature on process time in friction stir welding of Al 6061-T6," *Journal of Engineering*, vol. 2013, Article ID 580805, 5 pages, 2013.

[4] Y. Wei, H. Li, P. Xiao, and J. Zou, "Microstructure and conductivity of the Al-Cu joint processed by friction stir welding," *Advances in Materials Science and Engineering*, vol. 2020, Article ID 6845468, 10 pages, 2020.

[5] G. Pouget and A. P. Reynolds, "Residual stress and microstructure effects on fatigue crack growth in AA2050 friction stir welds," *International Journal of Fatigue*, vol. 30, no. 3, pp. 463–472, 2008.

[6] X. W. Yang, T. Fu, and W. Y. Li, "Friction stir spot welding: a review on joint macro-and microstructure, property, and process modelling," *Advances in Materials Science and Engineering*, vol. 2014, Article ID 697170, 11 pages, 2014.

[7] M. Cabibbo, A. Forcellese, E. Santecchia, C. Paoletti, S. Spigarelli, and M. Simoncini, "New approaches to friction stir welding of aluminum light-alloys," *Metals*, vol. 10, no. 2, p. 233, 2020.

[8] A. Andrzej, M. Korzeniowski, P. Kustroń, M. Winnicki, P. Sokołowski, and E. Harapińska, "Friction welding of aluminium and aluminium alloys with steel," *Advances in Materials Science and Engineering*, vol. 2014, Article ID 981653, 15 pages, 2014.

[9] W. M. Thomas and E. D. Nicholas, "Friction stir welding for the transportation industries," *Materials and Design*, vol. 18, no. 4–6, pp. 269–273, 1997.

[10] A. Abdollahzadeh, B. Bagheri, M. Abassi, A. H. Kokabi, and A. O. Moghaddam, "Comparison of the weldability of aa6061-T6 joint under different friction stir welding conditions," *Journal of Materials Engineering and Performance*, vol. 30, no. 2, pp. 1110–1127, 2021.

[11] N. Sharma, Z. A. Khan, and A. N. Siddiquee, "Friction stir welding of aluminum to copper-An overview," *Transactions of Nonferrous Metals Society of China*, vol. 27, no. 10, pp. 2113–2136, 2017.

[12] C. C. Sastry, P. Hariharan, and M. Pradeep Kumar, "Experimental investigation of dry, wet and cryogenic boring of AA 7075 alloy," *Materials and Manufacturing Processes*, vol. 34, no. 7, pp. 814–831, 2019.

[13] C. C. Sastry, P. Hariharan, M. Pradeep Kumar, and M. A. Muthu Manickam, "Experimental investigation on boring of HSLA ASTM A36 steel under dry, wet, and cryogenic environments," *Materials and Manufacturing Processes*, vol. 34, no. 12, pp. 1352–1379, 2019.

[14] J. C. Verduzco Juárez, G. M. Dominguez Almaraz, R. García Hernández, and J. J. Villalón López, "Effect of modified pin profile and process parameters on the friction stir welding of aluminum alloy 6061-T6," *Advances in Materials Science and Engineering*, vol. 2016, Article ID 4567940, 9 pages, 2016.

[15] A. Navukkarasan, M. P. Kumar, and C. C. Sastry, "Experimental investigation of dry and cryogenic broaching of AISI 4340 steel," *Materials and Manufacturing Processes*, vol. 35, no. 14, pp. 1584–1597, 2020.

[16] P. Jovičević-Klug and B. Podgornik, "Review on the effect of deep cryogenic treatment of metallic materials in automotive applications," *Metals*, vol. 10, no. 4, p. 434, 2020.

[17] A. Bansal, A. K. Singla, V. Dwivedi et al., "Influence of cryogenic treatment on mechanical performance of friction stir Al-Zn-Cu alloy weldments," *Journal of Manufacturing Processes*, vol. 56, pp. 43–53, 2020.

[18] Y. Kaynak, "Evaluation of machining performance in cryogenic machining of Inconel 718 and comparison with dry and MQL machining," *International Journal of Advanced Manufacturing Technology*, vol. 72, no. 5, pp. 919–933, 2014.

[19] C. C. Sastry, M. Abeens, N. Pradeep, and M. A. M. Manickam, "Microstructural analysis, radiography, tool wear characterization, induced residual stress and corrosion behavior of conventional and cryogenic trepanning of DSS 2507," *Journal of Mechanical Science and Technology*, vol. 34, no. 6, pp. 2535–2547, 2020.

[20] S. Mabuwa and V. Msomi, "Effect of friction stir processing on gas tungsten arc-welded and friction stir-welded 5083-H111 aluminium alloy joints," *Advances in Materials Science and Engineering*, vol. 2019, Article ID 3510236, 14 pages, 2019.

[21] K. Hariharan, C. Chandrasekhara Sastry, M. Padmanaban, and M. Gideon Ganesh, "Experimental investigation of bioceramic (Hydroxyapatite and Yttrium stabilized zirconia) composite on Ti6Al7Nb alloy for medical implants," *Materials and Manufacturing Processes*, vol. 35, no. 1, pp. 521–530, 2020.

[22] C. C. Sastry, K. Gokulakrishnan, P. Hariharan, M. P. Kumar, and S. R. Boopathy, "Investigation of boring on gunmetal in dry, wet and cryogenic conditions," *Journal of the Brazilian Society of Mechanical Sciences and Engineering*, vol. 42, no. 1, p. 16, 2020.

[23] S. Rajamanickam, J. Prasanna, and C. Chandrasekhara Sastry, "Analysis of high aspect ratio small holes in rapid electrical discharge machining of superalloys using Taguchi

and TOPSIS," *Journal of the Brazilian Society of Mechanical Sciences and Engineering*, vol. 42, no. 2, p. 99, 2020.

[24] K. Thirumavalavan, S. C. Chandrasekhar, A. M, R. Muruganandhan, and M. A. Muthu Manickam, "Study on the influence of process parameters of severe surface mechanical treatment process on the surface properties of AA7075 T651 using TOPSIS and Taguchi analysis," *Materials Research Express*, vol. 6, no. 11, Article ID 1165i1, 2019.

[25] V. P. Goutham Murari, G. Selvakumar, and C. S. Chandrasekhara, "Experimental investigation of wire-EDM machining of low conductive Al-SiC-TiC metal matrix composite," *Metals*, vol. 10, no. 9, p. 1188, 2020.